Dalton Transactions

Paper

A Cyanide-Bridged Di-Manganese Carbonyl Complex that Photochemically Reduces CO_2 to CO

Hsin-Ya Kuo,[a] Tia S. Lee,[a] An T. Chu,[a] Steven E. Tignor,[a] Gregory D. Scholes,[a] and Andrew B. Bocarsly*[a]

www.rsc.org/

Manganese(I) tricarbonyl complexes such as $[Mn(bpy)(CO)_3L]$ (L = Br, or CN) are known to be electrocatalysts for CO_2 reduction to CO. However, due to their rapid photodegradation under UV and visible light, these monomeric manganese complexes have not been considered as photocatalysts for CO_2 reduction without the use of photosensitizer. In this paper, we report a cyanide-bridged di-manganese complex, $\{[Mn(bpy)(CO)_3]_2(\mu\text{-}CN)\}ClO_4$, which is both electrocatalytic and photochemically active for CO_2 reduction to CO. Compared to the $[Mn(bpy)(CO)_3CN]$ electrocatalyst, our CN-bridged binuclear complex is a more efficient electrocatalyst for CO_2 reduction using H_2O as a proton source. In addition, we report a photochemical CO_2 reduction to CO using the dimanganese complex under 395 nm irradiation.

Introduction

It has been suggested that the continued use of fossil fuels will force these resources to become harder to afford prior to depletion.[1] To combat this issue, the electrochemical reduction of CO_2 has attracted much attention, since it can convert unutilized waste into a useful precursor such as CO or a renewable fuel like methanol.[2–5] Such transformations are thermodynamically uphill due to the high stability of CO_2.[4] This energy requirement can be met photochemically if an appropriate catalyst is available. To make such a process sustainable, the photochemical process must be driven by solar wavelengths available at the earth's surface, and the catalyst must be readily available. To date, using a photosensitizer containing a precious metal (Ir or Re) is a common way to shift the absorption region to solar wavelengths while also avoiding photodegradation of the catalyst. For example, $[Re(bpy)(CO)_3Cl]$ (bpy = bipyridine), which was first reported as a photo- and electrocatalyst for CO_2 reduction by Lehn et al.,[6] has been extensively studied for photocatalytic CO_2 reduction to CO.[7] Lehn and coworkers demonstrated that although photochemically active, $[Re(bpy)(CO)_3Cl]$ decomposes under the near-UV irradiation which is needed to carry out the desired chemistry. One strategy that partially avoids this decomposition process is the introduction of a second polypyridal coordination complex as a dye sensitizer, which shifts the photoaction spectrum of the system into the visible region. However, the absorption overlap of the dye sensitizer compound and the CO_2 reduction catalyst still leads to some photodegradation of the catalyst. Recently, a series of Re(I) complexes containing pyridyl N-heterocyclic carbene (NHC) complexes were reported by Huckaba et al. to function as photocatalysts for CO_2 reduction without the need for a dye sensitizer.[8] In terms of practical application, the use of earth-abundant metal complexes is more advantageous. However, there is only one report of a non-sensitized photochemical CO_2 reduction by a first row transition metal complex to date. This recent work presented a porphyrin-based iron catalyst that can reduce CO_2 to CO.[9]

In marked contrast to the extensive studies on Re(I)-based complexes as pure electrocatalysts, studies utilizing the analogous Mn polypyridyl complexes as molecular catalysts were not reported until 2011, when the electrocatalytic activity of $[Mn(bpy)(CO)_3Br]$ was noted by Bourrez et al..[10] One of the challenges of electrocatalysis using Mn polypyridine complexes is due to the extreme photosensitivity of such type of the complexes in solution, which causes nonproductive photodecomposition even under modest exposure to room light.[11–14] This chemistry not only makes electrocatalytic studies of these compounds challenging, but it rules out this class of complexes as possible photochemical reagents. Research groups, including ours have attempted to improve the photostability of the complex by substitution of a strong field ligand at the bromide site[15] or by chelating the Mn center with pyridylimidazole in place of 2,2'-bipyridine[16] with limited positive results. While these modifications significantly improved the stability of the complexes toward undesired photodecomposition, the detrimental photochemical pathways are not totally eliminated. As a result, few examples have been reported using Mn(I) complexes for the light-induced reduction of CO_2. To date, this issue has been alleviated by combining the Mn(I) catalyst with a Ru-based photosensitizer, thus, precluding direct irradiation of the Mn-based catalyst.[15,17–19]

While $[Re(bpy)(CO)_3Cl]$ can be used both as a photocatalyst and a photosensitizer in a single component system,[20] photochemical CO_2 reduction remains a challenge for the

[a] Princeton University, Department of Chemistry, Princeton, New Jersey, United States. E-mail: bocarsly@princeton.edu

† Electronic Supplementary Information (ESI) available. CCDC 1830691.

analogous single component Mn-carbonyl systems.[18] However, work carried out to date provides some clues to overcoming this challenge. The aforementioned ligand substitution of [Mn(bpy)(CO)$_3$Br] by a strong π-acceptor, CN^- for the Br^- ligand, has been reported to prevent the formation of the [Mn(bpy)(CO)$_3$]$_2$, since CN^- does not readily dissociate compared to Br^-.[15,16] We hypothesize that the difficulty of applying Mn-carbonyl complexes as photoreduction reagents may have to do with the rapid dimerization upon irradiation as a result of the Mn(I)→bpy(π*) (metal-to-ligand charge transfer, MLCT) transition. Excitation into this state eventually leads to loss of the axial ligand allowing the dimerization reaction to proceed. This is a known excited state deactivation process in the analogous Re-based system.[21]

The net positive effect of adding a cyanide ligand suggested that a photochemical system might be derived by developing a cyanide-bridged di-manganese complex, since the undesired dimerization could be shut down, while still favoring photo-induced electron transfer through a bridged-cyanide framework.[22–24] This approach is further supported by the prior report that an analogous Re binuclear complex photochemically convert CO_2 to CO.[25] Herein, we report the synthesis of a CN-bridged di-manganese complex, and find that this complex exhibits an excellent selectivity and efficiency in electrocatalytic CO_2 reduction. Importantly, we both explore the influence of CN ligation on photoevolution of Mn(I)-complexes and demonstrate the first example of the CN-bridged dimanganese complex as a photoreagent for reducing CO_2 to CO without the introduction of a separate molecular photosensitizer.

Results and discussion

Synthesis and characterization

The complex {[Mn(bpy)(CO)$_3$]$_2$(μ-CN)}ClO$_4$ (**1**) was synthesized based on a modification of the work by Riera.[26] The CN-bridged di-manganese complex (**1**) was synthesized by coupling [Mn(bpy)(CO)$_3$Br] (**2**) and [Mn(bpy)(CO)$_3$CN] (**3**), as shown in Fig. 1a. We replaced the $TlPF_6$ reagent in Riera's synthesis with $AgClO_4$ and obtained the complex **1** with a yield of 75%. The product was characterized by UV-Vis, NMR, and FTIR spectroscopies. In addition, we also optimized the known synthesis of the CN-ligated precursor **3**,[26] obtaining a yield of 98% by reducing the reaction time to 1 h.

The UV-Vis absorption spectrum for the complexes **1**-**3,** as shown in Fig. 1b, exhibits a broad peak in the near visible region corresponding to a Mn(I)→bpy(π*) charge transfer absorption. In acetonitrile (MeCN), the CN-bridged product **1**, the Br-ligated reactant **2**, and the CN-ligated reactant **3** display absorption at 364 nm (ε = 10,810 dm^3 mol^{-1} cm^{-1}), 417 nm (ε = 3,874 dm^3 mol^{-1} cm^{-1}), and 375 nm (ε = 4,100 dm^3 mol^{-1} cm^{-1}), respectively. The absorption maxima of complex **1** is blue-shifted with respect to complex **2** and **3** by 53 and 11 nm, respectively. The presence of the strong cyanide ligand (complexes **1** and **3)** results in a higher energy MLCT transition compared to complex **2,** which lacks a cyanide ligand. The smaller shift in the MLCT between **1** and **3** is attributed to the different binding properties of the two ends of cyanide.[27]

The IR absorption spectra of complexes **1**-**3** in MeCN are shown in Fig. 1c and the solid-state ATR-IR of the three complexes are also included in Fig. S1†. In the ATR-IR spectra, **1**-**3** demonstrate three intense carbonyl stretching bands between 1,900 and 2,500 cm^{-1}, which is consistent with the facial arrangement of the three carbonyl groups. The two bands at lower wavenumbers result from the symmetric and antisymmetric stretching vibrations of the two equivalent COs that are trans to the bipyridine ligand.[28,29] The remaining band at the highest frequency corresponds to the stretching mode of the axial CO, which is trans to the halide (or pseudohalide) ligand (i.e., Br or CN).[28,29] Compared with the CO stretching bands of the Br-coordinated **2**, the CN-ligated complexes **1** and **3** show a slight shift to higher wavenumbers. This shift is consistent with a decrease in the π* donation to the carbonyl carbon in the presence of a strong π-acceptor (i.e. cyanide). One striking feature of **1**, shown in Fig. 1c, is that two CO ligands lying on the complex's principle axis (trans to the cyanide ligand) are energetically inequivalent forming an accidental doublet peak centered at 2,042 cm^{-1}. The inequivalence of these two CO stretches can be attributed to the different binding properties of the C- and N- terminals of the cyanide, as will be discussed later. Moreover, the cyanide IR stretching frequencies allow differentiation of the terminal CN linkage from the bridged one. The terminal CN stretch of **3** is observed at 2,108 cm^{-1} whereas the bridged cyanide complex **1** yields a cyanide stretch at 2,147 cm^{-1}, which is in good agreement with literature,[24,26,30–32] and the increase in the bridging cyanide frequency is due to kinematic coupling.[33,34] The cyanide and carbonyl stretching frequencies of **1** are similar to the CN-bridged Re analog.[35,36]

The carbonyl resonances region of **1** in the $^{13}C\{^1H\}$ NMR spectrum provides conclusive support for the existence of two distinct axial CO ligands and two different Mn centers (see Fig.

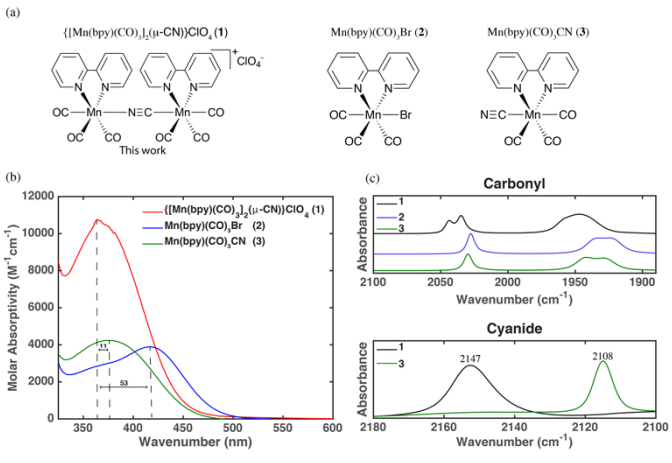

Fig. 1 (a) Representation of the complexes **1**-**3**. (b) UV-Vis absorption spectra of complexes **1**, **2**, and **3** in MeCN at 298K at 1 cm path length show MLCT band positions. CN-ligated complexes **1** and **3** display higher energy MLCT band compared to Br-ligated complex **2**. Smaller difference in MLCT position between **1** and **3** reflect different binding properties of the two ends of CN. (c) Carbonyl and cyanide regions are represented in the infrared spectra of **1**-**3** in MeCN.

S11†). Two overlapping signals in the downfield region are observed at 220.4 and 220.1 ppm, which are associated with the axial carbonyls perpendicular to the bpy planes. Two equatorial carbonyl resonances occur at 217.3 and 212.7 ppm and this suggests that the two sets of *cis*-COs are slightly different. Therefore, the distinguishable equatorial CO peaks support the presence of two different Mn nuclei resulting from the bridged CN linkage. The carbonyl shifts agree well with the reported CN-ligated **3**.[32,37] We also note that the bridged CN resonance occurs at 170.0 ppm, which is 9 ppm more downfield than the terminal CN resonance in **3,** consistent with the formation of a linear bridging ligand.[32]

Complex **1** was recrystallized in a mixed solvent of CH_2Cl_2-*n*-hexane to generate a diffraction quality single crystal. Single crystal x-ray diffraction analysis of this sample yielded the structure provided in Fig. 2a. The two [Mn(bpy)$(CO)_3$] fragments are bridged by a cyanide in a nearly linear fashion with a bond angle of 174°±2° relative to the OC-Mn-CN-Mn-CO principle molecular axis. The μ-CN bond length is 1.152 Å, similar to other bridged-cyanide complexes.[26] In addition, the shorter Mn-C distance in comparison to Mn-N (1.990 Å vs 1.998 Å) is consistent with back-bonding on the C-side of the cyanide ligand. The conformation as shown in Fig. 2b is quite intriguing: there is a nearly complete eclipse along the Mn-CN-Mn axis with the two bpy planes tilted toward each other by 2° and 5°, respectively. The distortion is more pronounced for the bpy moiety on the N-end of cyanide. The shortest distance between the bpy rings is 3.702 Å suggesting a weak π-π attraction between these rings. This interesting conformation also has been reported in the analogous cyanide bridged Re complex;[30] however, the closely related {[Mn(1,10-phen)$(CO)_3]_2$(μ-CN)}$^+$ adopts a trans conformation.[26] We suspect that the eclipse conformation can be attributed to a combination of packing forces and the suggested π–π interaction. Temperature dependence of ^{1}H-NMR over a wide range of temperatures (251-318 K) indicated no signal broadening of the bpy hydrogens suggesting free rotation along the Mn-CN-Mn for the dissolved complex, thus, supporting the idea that packing forces play a role in the observed x-ray structure conformation (see Fig. S2†).

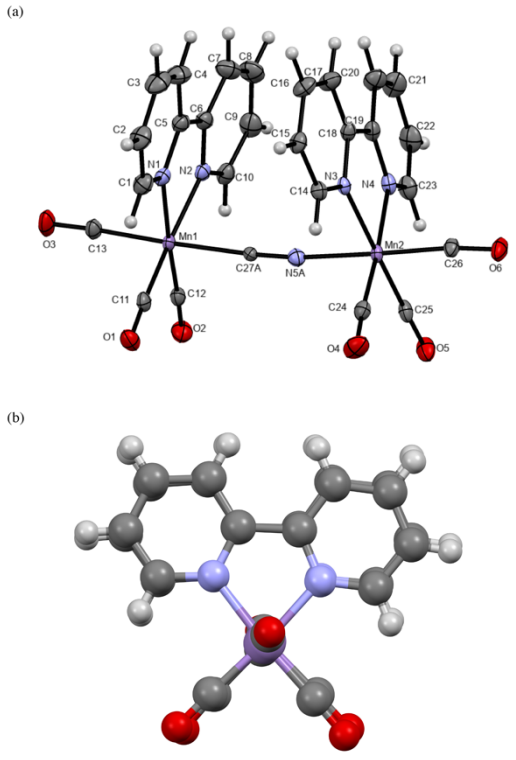

Fig. 2 (a) Molecular structure of **1**; ellipsoids are set at 50% probability. CH_2Cl_2 and ClO_4 have been omitted for clarity. Selected bond lengths [Å]: Mn1–C27A 1.990(2), Mn1–C13 1.841(3), C13-O3 1.141(3), C27A–N5A 1.152(3), Mn2–N5A 1.998(2), Mn2-C26 1.818(2), O6-C26 1.146(3), Mn1–C11 1.811(2), O1–C11 1.148(3), Mn2–C24 1.808(2), O4–C24 1.146(3). (b) Eclipsed conformation {[Mn(bpy)$(CO)_3]_2$(μ-CN)}$^+$ down the principle molecular axis.

Electrochemistry

Cyclic voltammetry (CV) of the mononuclear parent complexes and the binuclear complex allow the identification of several of the observed reduction waves. Fig. 3a shows the CV data at 250 mV/s for complex **1**-**3** in MeCN with 0.1 M tetrabutylammonium perchlorate (TBAP) under argon. The binuclear complex **1** shows four reduction waves (black trace); the two most positive reduction waves, observed at peak potentials of -1.68 V and -1.85 V vs Fc/Fc$^+$ are non-reversible (i.e. no return waves are evident) over the scan rates ranging from 25 mV/s to 1000 mV/s (see Fig. S3†). By analogy to {[Re(bpy)$(CO)_3]_2$(μ-CN)}PF_6,[31] these two waves are assigned to the reduction of the bpy ligands attached to the two Mn(I) centers. The lack of reversibility suggests follow up chemical reactions occur after each reduction. The third reduction produces a pair of peaks with $E_{1/2}$ = -1.92 V vs Fc/Fc$^+$ and peak-to-peak separation over the applied scan rates indicative of a quasi-reversible process (see Fig. S4†). This third redox process and the first reduction of the terminal CN-ligated complex **3** both occur at nearly identical potentials and demonstrate comparable reversibility as measured by the Nicholson and Shain diagnostics (see Fig. S4†).[38] Therefore, it appears that a fraction of the bridged dimer dissociates forming the terminal cyanide monomer after the second reduction wave and that the third redox couple is addition of an electron to the π*-orbital of the bpy ligand in this monomeric unit.[37] However as discussed later, this decomposition reaction only occurs when dry and CO_2-free MeCN is employed as the electrolyte. The stability of the bridging cyanide ligand is dramatically enhanced in the presence of CO_2 and a proton source. At more negative potentials, a fourth irreversible reduction wave peaked at -2.49 V vs Fc/Fc$^+$ is tentatively assigned to the reduction of [Mn (bpy$^{-\cdot}$)$(CO)_3$CN] followed by cyanide loss based on the observation that this wave is observed for both complex **1** and **3**.[37] The return scan of complex **1** displays three oxidation peaks: -1.88 V, -1.50 V, and -0.61 V, vs Fc/Fc$^+$. The two most negative oxidation waves are absent if the potential is switched before the third quasireversible process as shown in Fig. 3b. Since the most negative oxidation peak is the anodic portion of the bpy reduction wave, this peak is assigned to the re-oxidation of the monomeric CN-Mn complex. The next most positive wave

represents a non-reversible oxidation, which can be associated with the monomeric cyano-Mn complex based on the data in Fig. 3b. This peak is assigned to the oxidation of $[Mn(bpy)(CO)_3]^-$, generated via the cyanide loss from $[Mn(bpy)(CO)_3CN]^-$ at the fourth irreversible reduction, followed by the formation of $[Mn(bpy)(CO)_3]_2$.[10,37] The most positive anodic peak, by analogy with the mononuclear parent complexes, is assigned to the oxidation of the Mn-Mn dimer formed from the monomeric reaction products.[10]

Since the pioneering study of $[Mn(bpy)(CO)_3Br]$ (**2**) as an electrocatalyst for CO_2 reduction described by Deronzier et al.,[10] Mn-based complexes with various polyaromatic derivatives have been examined to probe the selectivity and efficiency of

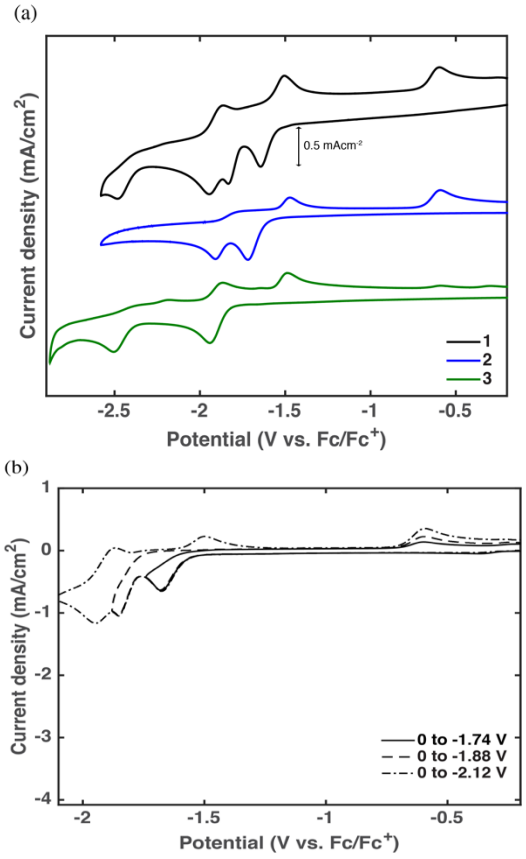

Fig. 3 (a) CV data of complex **1**-**3** (1mM) using 0.1 M TBAP in MeCN under Ar-atmosphere at 250 mV/s using a 3 mm glassy carbon working electrode, a platinum foil counter electrode and a Ag/Ag^+ non-aqueous reference electrode. All potentials are referenced to Fc/Fc^+. (b) CV data of complex **1** at various switching potentials using a scan rate of 250 mV/s. Other conditions are the same as Fig. 3a.

CO_2-to-CO in this system.[37,39–42] In contrast to the Re analogs, Mn-based catalysts typically require the use of a proton source such as H_2O. To examine the binuclear complex's ability to reduce CO_2, the complex was evaluated using CV in CO_2-saturated electrolyte with and without addition of a proton source as shown in Fig. 4a. Upon addition of 5% H_2O into the CO_2-saturated electrolyte, the oxidation waves centered at -1.50 V and -0.61 V vs Fc/Fc^+ both disappear, and an enhancement of the cathodic current (1.3X) at the second reduction peak was observed as shown by the dashed line; both phenomena suggest that CO_2 reduction is catalyzed by the

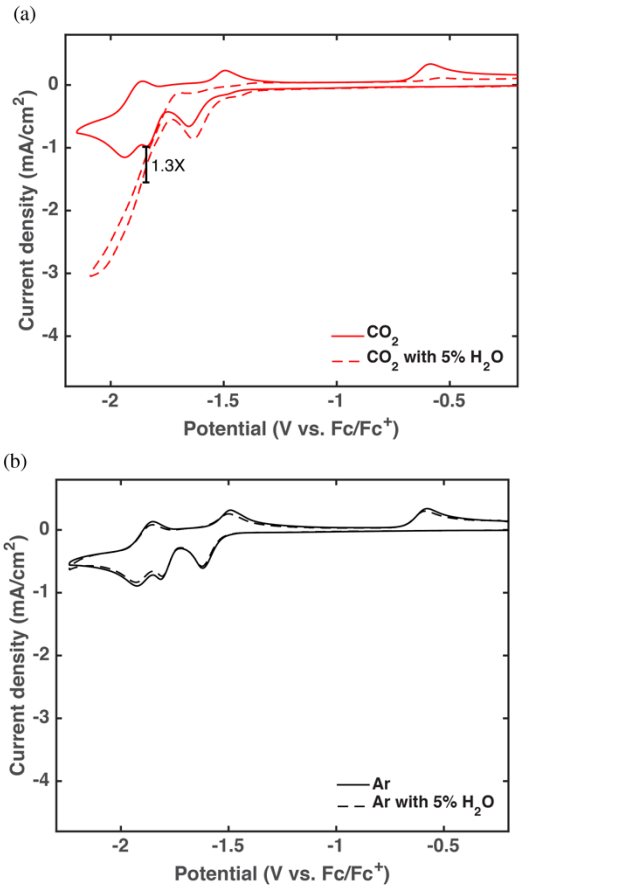

Fig. 4 CV data of complex **1** with and without 5% H_2O under CO_2 atmosphere (a) and Ar atmosphere (b) at a scan rate of 250 mV/s. All other conditions are the same as given in Fig. 3.

species associated with the second reduction of **1**. Additionally, upon addition of water the shape of the first reduction wave significantly changes with a slight current increase under CO_2 while no significant change exists in the wet electrolyte under Ar as shown in Fig. 4b. The effect of H_2O content on catalytic activity was investigated by monitoring the current at -1.85 V vs Fc/Fc^+ upon addition of H_2O. Addition of H_2O from 5% to 15% by volume did not lead to a higher current at the second reduction peak (Fig. S5a†) indicating that at 5% water, the proton demand was saturated.[39]

Although higher catalytic current can be observed at more negative potentials than the second reduction peak, there is an uncertainty regarding the stability of the CN-bridged structure at these potentials, and thus, alternative reaction pathways may be involved complicating the catalysis. To alleviate unwanted CN-bridged cleavage bulk electrolyses were carried out at -1.90 V vs Fc/Fc^+. The system was found to be stable for extended periods at this potential in the presence of 5% H_2O and CO_2. Electrolysis for 4 h, monitored by gas chromatography (GC) headspace analysis identified CO as the reaction product. The product analysis in Fig. S5b† shows that the amount of CO produced is directly proportional to the charge passed, with a maximum Faradaic efficiency (FE) of 90% and an average FE of 73% over a 4 h observation period. This result demonstrates that the observed current enhancement is due to the reduction

of CO_2 to CO. The CN-bridged catalyst **1** displays a high selectivity for CO production with the balance of the charge passed being associated with H_2 evolution directly from the electrode surface. No soluble organic products including formate were found in the ^{1}H NMR of the post bulk electrolysis electrolyte (Fig. S6†). The stability of **1** during electrolysis was evaluated by taking CVs every 20 min during the electrolysis. The first reduction wave centered at -1.70 V vs Fc/Fc^+ was determined to be diagnostic for the integrity of the intact bridged-CN linkage. As shown in Fig. 5, while the cyanide bridge degraded relatively rapidly in the absence of CO_2 and H_2O, it was quite stable during CO_2 reduction — only a 15% CV peak current drop was observed over 4 h and the system maintained a steady bulk electrolysis current density (~0.8 mA/cm^2).

We selected the FE for CO production for each complex as a figure of merit (Table 1) to compare the catalytic efficiency of **1** with the known catalysts **2** and **3**. Our CN-bridged catalyst demonstrates similar efficiency for CO formation when compared with the Br-ligated precursor **2**.[39] The electrochemistry of complex **1** was compared to the CN-ligated monomer **3** utilizing 5% H_2O as a proton source. Bulk electrolysis with **3** held at -2.50 V vs Fc/Fc^+ yields an average FE of 40% for CO production (~50% for H_2 production) while complex **1** retained a FE of 75% for CO at -1.90 V vs Fc/Fc^+ passing the same amount of charge (16 C) in both cases. Despite the fact that **3** catalyzes CO_2 to CO, the negative potential needed to carry out this process results in the competitive reduction of water directly at the glassy carbon electrode. Since, using **1** as an electrocatalyst for CO_2 reduction in wet electrolytes can efficiently produce CO at less negative potential, the unwanted H_2 side reaction is significantly inhibited.

In addition to evaluating each complex's FE for CO formation, we compared another performance parameter--catalytic efficiency (ξ_{cat}). The ξ_{cat} parameter provides an approach to assess each complex's activity toward CO_2 reduction based on both overpotential and partial current density.[43] The partial current density, j_{prod}, is the observed current density times the FE for the product of interest, and is a measure of the catalytic turnover frequency. This parameter allows comparison of different catalysts in a mechanistically independent manner. The catalytic efficiency is a power density ratio described in Eq. (1):

$$\xi_{cat} = \frac{j_{prod}E^{o'}_{prod}}{j_{total}E_{appl}} = FE\frac{E^{o'}_{prod}}{E^{o'}_{prod}-\eta} \qquad (1)$$

where j_{total} the overall current density, $E^{o'}_{prod}$ the formal redox potential of the reaction, E_{appl} the experimentally applied potential and η the overpotential. As catalyst efficiency improves, (i.e. the smaller η and the higher partial current density) ξ_{cat} moves toward unity. In the present work, $E^{o'}_{prod}$ for CO formation is -1.28 V vs Fc/Fc^+ in nonaqueous media (5% H_2O in MeCN),[44] producing the ξ_{cat} values listed in Table 1. The similarity in performance between **1** and **2** demonstrates that the CN-bridged **1** is a promising electrocatalyst in wet electrolytes with good selectivity. However, the CN-ligated monomer **3** operated in the wet electrolyte yields poor catalytic efficiency due to the large overpotential and poor selectivity for CO formation compared with the competing hydrogen evolution reaction.

The proposed reaction mechanism of **1** upon reduction (Eqs. 2-4) is supported by digital simulation of the CV curves. Fig. 6 shows a representative fit of the experimental and simulated CV data at 250 mV/s. Simulation results over the scan rate ranges of interest are included in Fig. S7†. In this discussion, we consider only the first two reduction processes observed in the CV since they are both associated with intact complex **1**.

The first reduction process at -1.68 V vs Fc/Fc^+ is ascribed to a bpy-based reduction as given in Eq. (2), which is formally represented as $\mathbf{Mn}^-$. A standard redox potential of -1.65 V vs Fc/Fc^+ is estimated by digital simulation. The irreversibility of the first reduction process indicates a chemical reaction. That is, we suggest that reduction of the bpy moiety is followed by an internal charge transfer to move the electron into the d-orbital manifold. Then, Eq. (3) hypothesizes an electrochemically induced CO dissociation followed by the rapid MeCN coordination to yield $\mathbf{MnA}^-$.[45]

The second reduction process shown in Eq. (4) at -1.85 V Fc/Fc^+ is ascribed to the one-electron reduction of the second bpy-ligand to form $\mathbf{MnA}^{2-}$, with an estimated standard redox potential of -1.80 V vs Fc/Fc^+. Note that in the CV data does not evidence a return wave for the reoxidation of either $\mathbf{MnA}^-$ or $\mathbf{MnA}^{2-}$, independent of the scan rates employed (Fig. S7†). Therefore, $\mathbf{MnA}^-$ and $\mathbf{MnA}^{2-}$ are never in equilibrium at the electrode suggesting that they are both unstable in the solution. Moreover, based on the CV shown in Fig. 4a, the current enhancement is associated with the CO_2 reduction coupled with $\mathbf{MnA}^{2-}$.

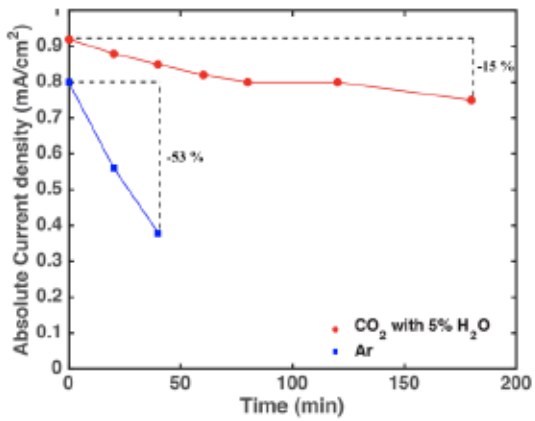

Fig. 5 Absolute peak current density at the first reduction wave (-1.70 V vs Fc/Fc^+) versus time over the course of a bulk electrolysis at -1.90 V vs Fc/Fc^+. Data were collected with solutions of **1** (1 mM) in CO_2-saturated 0.1 M TBAP/ MeCN with 5% H_2O (red) or in Ar-saturated dry electrolyte (blue). Under Ar, the peak current density rapidly decreased during the first 40 min and was absent after 1 hour, indicating degradation of **1**. While **1** yielded good electrochemical stability in CO_2 wet electrolyte with only a 15 % peak current drop.

Table 1. Efficiency Comparison of Complex **1**-**3** for the reduction of CO_2 to CO

Complex	FE_{CO} [a] (%)	$E^{o'}_{prod}$ [b] (V)	E_{appl} [b] (V)	η [c] (V)	ξ_{cat}
{[Mn(bpy)(CO)$_3$]$_2$(μ-CN)}ClO$_4$ **1**	73	-1.28	-1.90	0.61	0.49
[Mn(bpy)(CO)$_3$Br] **2** [d]	75	-1.28	-1.88	0.60	0.51
[Mn (bpy)(CO)$_3$CN] **3**	40	-1.28	-2.59	1.20	0.20

[a]Each entry is the average FE obtained from a 4 h bulk electrolysis. [b]Potential vs Fc/Fc^+. [c]Each overpotential is calculated by the difference between the formal redox potential and the applied potential. [d] From Ref. 3

$$[Mn{-}C{\equiv}N{-}Mn]^+ \xrightarrow[-1.68\ V]{+\,e^-} [Mn{-}C{\equiv}N{-}Mn]^{\cdot} \qquad (2)$$
1 **Mn$^-$**

$$[Mn{-}C{\equiv}N{-}Mn]^{\cdot} \xrightarrow[+MeCN]{-CO} \text{solvato complex} \qquad (3)$$
Mn$^-$ **MnA$^-$**

$$\mathbf{MnA^-} \xrightarrow[-1.85\ V]{+\,e^-} \mathbf{MnA^{2-}} \qquad (4)$$

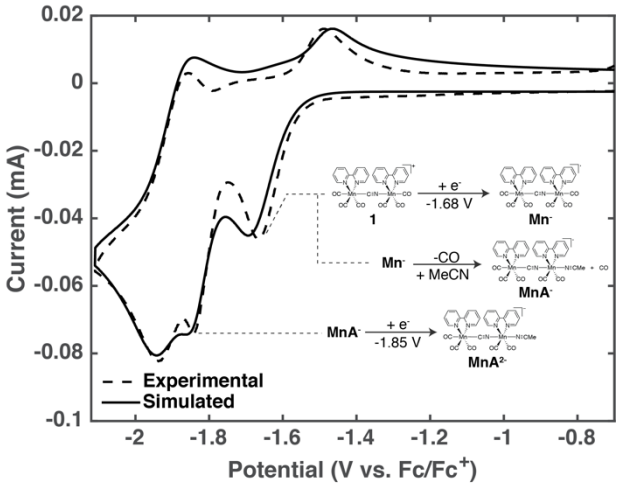

Fig. 6 Comparison of simulated and experimental CV data of complex **1** using 0.1 M TBAP in MeCN under Ar-atmosphere at a scan rate of 250 mV/s. A 3 mm glassy carbon electrode was used as a working electrode. In the simulations, we excluded any data more positive than -0.9 V vs Fc/Fc+. The reductive features are described in the text.

Photochemistry

As already noted, the use of single Mn complexes such as compounds **2** and **3** to photochemically convert CO_2 into CO is untenable due to the extent of rapid photodegradation of these complexes. Nonetheless, the photophysics leading to the primary photochemical product from these mononuclear complexes can be studied. Such a study was carried out to evaluate the influence of the terminal cyanide ligand. To that end, we examined the photochemistry of complexes **2** and **3** in MeCN by monitoring the change of the compounds with UV-Vis spectroscopy upon direct excitation into the Mn→bpy MLCT band. The variations in the UV-Vis spectra of the complex **2** and **3** are shown in Fig. 7a and b, respectively. For the Br-ligated complex **2**, the MLCT band at ~420 nm shows blue-shifted characteristics over the reaction period. In addition, we observe new features between 600–900 nm which are attributed to the formation of a Mn-Mn bonded dimer, i.e. $Mn_2(CO)_6(bpy)_2$. These observations are consistent with previously reported work by Stor and coworker.[11,12] In contrast to **2**, the complete absence of the aforementioned peaks between 600–900 nm in the CN-ligated complex **3** suggests successful prevention of dimerization by replacement of Br^- ligand with CN^- (Fig. 7b).

The photochemistry of the CN-bridged complex **1** was examined under the same experimental conditions, with the results presented in Fig. 7c. As observed for complex **3**, the 600–900 nm region of the spectrum remains clear during the photolysis confirming the absence of Mn–Mn bond formation. Additionally, both complex **1** and **3** exhibit gradual spectral restructuring in 300–600 nm, where a diminished MLCT band ~370 nm is accompanied by the rise of a transition observed as a shoulder peaking at ~520 nm. Clear isosbestic points were observed ~420 nm for both complexes **1** and **3**. The presence of the isosbestic point indicates conversion of the reactant complex into a single photo-induced product. The spectral features that have been previously attributed to Mn-Mn metal bonded dimer were not observed.[11,12] In the photolysis of complex **3**, we propose formation of a photoproduct resulting from CN loss followed by an MeCN ligation.[15] The nature of the photoproduct of **1** will be discussed later.

To gain additional insight into nature of the photo-product, we carried out the irradiation of **1** in the weakly coordinating solvent, 2-MeTHF. The results are provided in the Fig. 7c (inset). The MLCT band of **1** at 364 nm in 2-MeTHF does not shift in energy or intensity over a 1 h photolysis. Thus, photolysis of complex **1** in 2-MeTHF is strikingly different from that in MeCN. Notably, in 2-MeTHF, we did not observe an isosbestic point. This argues for participation of MeCN as a ligand in a photo-induced intermediate. While CO substitution by 2-MeTHF has been described in Mn carbonyl complexes at low temperture,[46–49] coordination between **1** and 2-MeTHF is expected to be unfavorable at room temperature, consistent with the absence of an isosbestic point during the photolysis of **1**.

To verify the integrity of the bridged-CN bond upon irradiation into the MLCT band, the photolysis of **1** in MeCN with 365 nm 3W LED was monitored using IR spectroscopy, as shown in Fig. 8a (for the cyanide and carbonyl stretching region). The bridged-CN band shifts slightly to lower energy from 2,150 to 2,138 cm^{-1} (Fig. 8a, inset), which is consistent with an intact CN-bridged Mn complex.[26] The higher frequency CO-stretching bands are associated with the two axial COs lying along the

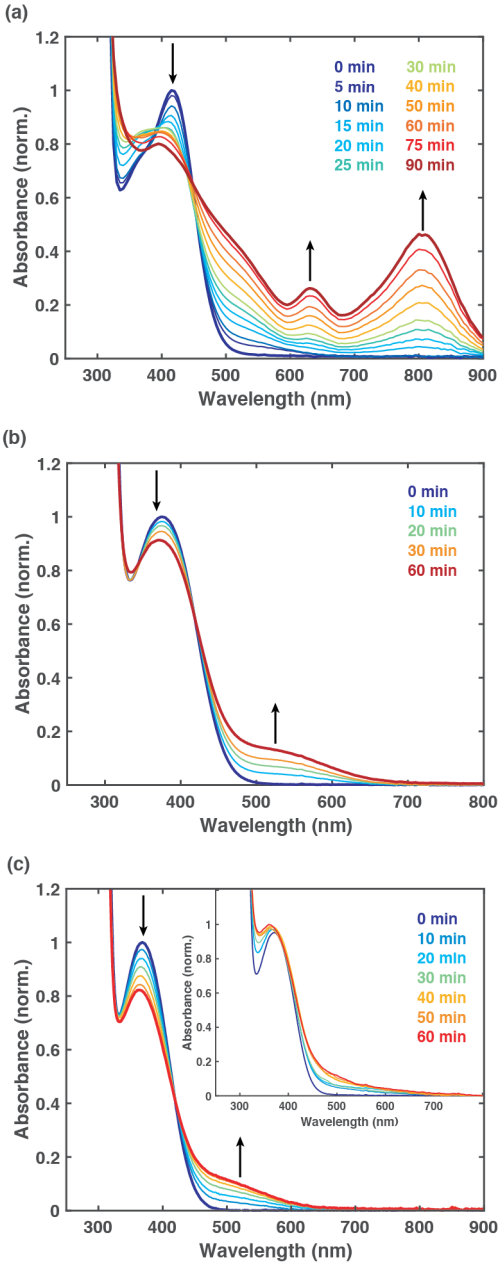

Fig. 7 Evolution of UV-Vis absorption spectra of (a) **2** and (b) **3** in stirred MeCN at 298 K upon irradiation with a 365 nm pulsed laser. (c) Photoresponse of **1** in MeCN and 2-MeTHF (inset), respectively, and all the other experimental conditions are kept fixed.

molecules principle axis. Of these two bands, the higher frequency band is observed to disappear, while the lower energy band remains constant (2,037 cm^{-1}). We hypothesize that the CO trans to the C-end of the cyanide ligand dissociates upon photolysis. This is in line with the binding inequivalence of the two COs, which has been discussed previously. The vacant site is then filled by an MeCN leading to the formation of the photoproduct, and consistent with the isosbestic point observed in Fig. 7c. To confirm this chemistry, **1** was photolyzed in the presence of triphenylphosphine (PPh_3) in acetonitrile. The product was analyzed using ^{31}P NMR. A broad signal at 30.3 ppm was observed confirming the ligation of PPh_3 at an axial CO site (Fig. S8a†). The reaction was monitored using FTIR spectroscopy (Fig. S8b†). As in the prior case, where PPh_3 was not present, one of the axial COs was observed to disappear; further supporting the described photo-induced CO dissociation. Additionally, the FTIR spectrum of the phosphine substituted photoproduct indicates that the bridged-CN is present in this species. We also considered a possible degradation route: the CN-cleavage may occur between Mn and N-end of the CN bond based on lengthened Mn-N bond observed in the crystal structure; the resulting products may include CN-ligated monomer **3**, the solvated $[Mn(bpy)(CO)_3(MeCN)]PF_6$ and $Mn_2(CO)_6(bpy)_2$. The photolysis experiments (Fig. 7c) allow us to exclude the possibility of Mn-Mn dimer formation. The IR spectrum of **1** after 4 min irradiation is overlaid with that of **3** and $[Mn(bpy)(CO)_3(MeCN)]PF_6$ in Fig. 8b. This data clearly show that the patterns of the photo-induced products are different from the two hypothesized intermediates; therefore, the proposed degradation route is excluded. The available data support the robustness of the CN-bridged structure of **1** under the employed photolysis conditions.

As previously mentioned, the dimerization is known to be a deactivation process in the analogous Re-based system;[21] furthermore, the electrochemical formation of a Mn-Mn bonded dimer is inhibited by replacing the bromide ligand with a cyanide as reported by Kubiak and coworkers,[15,37] which is indeed observed in the aforementioned photolysis of **1** and **3**. The inhibition of dimer formation suggests that it might be possible to photochemically bind and activate CO_2 reduction using either complex **1** or **3**. To test this hypothesis, we loaded

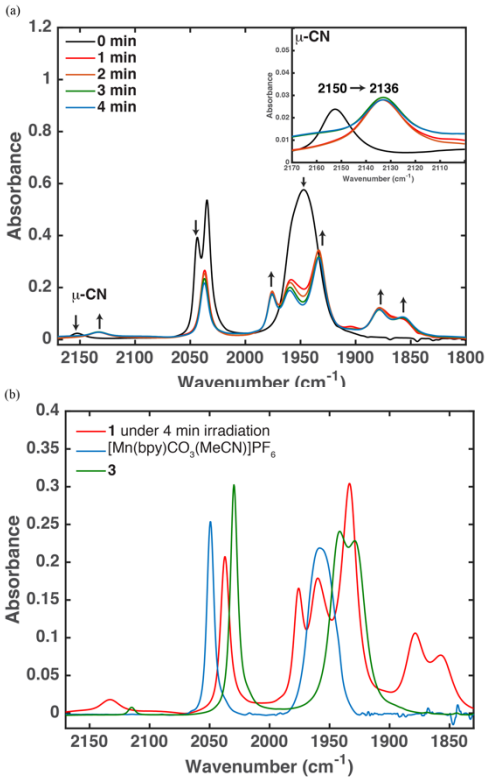

Fig. 8. IR spectral changes upon photolysis of 20 mM **1** (a) in MeCN with 365 nm LED light (see experimental section for details). Changes of cyanide (inset) and carbonyl stretching bands are indicated with arrows. (b) The IR spectrum upon 4 min irradiation of **1** (blue trace in Fig. 8a) is compared with that of **3** and $[Mn(bpy)CO_3(MeCN)]PF_6$ (keeping all the other conditions fixed).

Table 2. Comparison of Photolysis Yields Under 395nm Irradiation

Entry	**1**/μMol	Proton Source	CO/μMol[b]	ϕ_{CO}[b]
1[a]	8.0	H_2O 5%	1.6	0.65
2[a]	8.0	PhOH 1M	2.2	0.85
3[c]	8.0	0	0.0	-

[a]A 15-mL vial containing 1 mM **1**, proton source and 8 mL MeCN was vigorously bubbled with CO_2 in the absence of light and irradiated with 395 nm 3W LED for 10 min. The light intensity was 5.2×10^{-9} E s^{-1}. [b]The quantum yield is calculated from the mol of detected CO divided by the Einsteins of photons absorbed. [c]This run was conducted as a dark control.

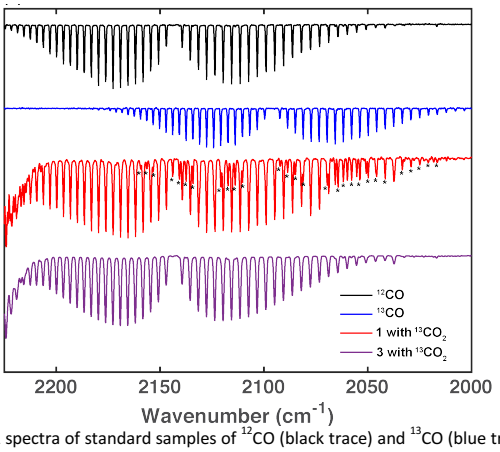

Fig. 9. FT-IR spectra of standard samples of ^{12}CO (black trace) and ^{13}CO (blue trace) to our headspace samples (red and purple traces for **1** and **3**, respectively); see experimental section for details. In case of **1**, the headspace sample yields a mixture of ^{12}CO and ^{13}CO (black stars), while the sample from **3** contains only ^{12}CO.

1 mM of each complex in a sealed borosilicate glass reactor containing $^{13}CO_2$-saturated with 5% H_2O (v/v) as a proton source. After 20 min of irradiation with 395 nm monochromic light, 9.1 μmol of CO were detected from the headspace sample of the vial containing **1** without H_2 formation. The reactor headspace was analyzed by IR spectroscopy as depicted in Fig. 9. The appearance of ^{12}CO indicates the loss of CO ligands from **1** which contains six ^{12}CO ligands. The existence of ^{12}CO has also been observed in the electrocatalysis of CO_2 reduction using the parent complex **2**.[39] The presence of ^{13}CO confirms that the ability of the CN-bridged **1** to photochemically reduce CO_2 to CO.

There is a striking difference between complexes **1** and **3** in their photochemical reaction with $^{13}CO_2$ as portrayed by the IR data in Fig. 9. The headspace sample from the vial containing **1** yields both ^{13}CO and ^{12}CO, while the vial containing **3** only gives 3.2 μmol ^{12}CO. In both cases H_2 is not observed. Thus, the CN-bridged binuclear **1** carries out the photon-assisted CO_2 reduction to CO, while the mononuclear, CN-ligated **3** only undergoes CO dissociation.

It is important to recognize that while the observation of a pure ^{12}CO product during the photolysis of complex **3** can only be explained by the photochemical decomposition of **3**; the mixed ^{13}CO/^{12}CO product stream observed during the photolysis of complex **1** does not indicate that a decomposition pathway is operating. In the latter case, all of the CO ligands are more or less kinetically equivalent including the CO ligand formed upon reduction of the bound CO_2, and thus, one might reasonably anticipate as much as a 1:6 ratio of ^{13}CO/^{12}CO early in the product stream formed from a stable photoactivated form of **1**.

As shown in Table 2, irradiation into the MLCT band of complex **1** in the presence of CO_2, and a proton source produces CO with a quantum yield between 0.5 and 1. The actual value is dependent on the quantity and source of protons. While the lack of a proton source shuts down CO photoproduction, once 1 M of a source is present (given 1mM complex **1**) the reaction is saturated in protons. It is observed that the source of protons has a large impact on the observed quantum yield. This phenomenon remains under investigation.

Photolysis studies were carried out over relatively short periods of time, since the conditions employed were stoichiometric in the chromophore. A true catalytic cycle would require the presence of a sacrificial reductant to restore the complex's oxidation state. Thus, in order to study the fundamental photoinduced charge transfer chemistry of this system, only initial reactivity was analyzed. However, evaluation of the integrity of the complex using UV-Vis spectroscopy (see Fig. S9†) indicated a high degree of stability.

No evidence of absorbance in the 600-800 nm region indicates that a Mn-Mn bonded dimer is not formed, and suggests that the cyanide bridge remains intact. A new band is observed ~500 nm, which we assign to a MLCT transition in a cyanide bridged dimer complex having an axial MeCN ligand in place of the initial CO ligand based on our earlier discussion (see Fig. 7), and as expected if CO_2 is ligated, reduced (to CO) and then released. Thus, the initial photoprocesses indicate that the complex core remains intact and efficiently reduces CO_2 to CO with a high quantum yield when excess protons are present. We suggest this bodes well for the future development of a photocatalytic cycle based on a cyanide bridged manganese dimer system.

Conclusions

We present a new CN-bridged Mn binuclear complex that acts both as an electrocatalyst and a photochemical reagent for CO_2 reduction to CO. Single crystal X-Ray crystallography revealed that the cyanide bridged complex **1** has a unique eclipsed conformation in the solid state. The complex is found to have an onset potential for CO_2 reduction that is 700 mV less negative then that observed for the CN-ligated precursor; Unlike the Br-ligated precursor, the dimer system presented here shows increased resistance to undesirable and destructive photo dimerization. The CN-ligated precursor exhibited no photochemical activity for CO_2 reduction. In contrast, the CN-bridged binuclear Mn complex facilitates the photochemical

reduction of CO_2 to CO. Future studies are planned to develop a system that continually photoreduces CO_2 using either a sacrificial reductant or a combined electrochemical/ photochemical cycle based on the CN-bridged binuclear Mn complex's chemistry reported here.

Experimental section

General Procedures

Synthetic reactions were conducted using standard Schlenk-line techniques under an atmosphere of argon. For all electrochemical experiments, the electrolyte was bubbled with the desired gas (Ar or CO_2) for 15 min prior to taking a background scan to ensure a featureless background from 0 to −2.9 V vs Fc/Fc^+. After adding the desired complex, the electrolyte was bubbled for additional 5 min prior to data collection. Complexes were loaded at a concentration of 1 mM for both CV and bulk electrolysis. Ferrocene was added as internal reference. The total volume of electrolyte used for these experiments was 10 mL for CV and 25 mL for bulk electrolysis. Bulk electrolyses were operated for ~4 h, and the headspace was analyzed by GC approximately every 20 min. The proton concentration was kept consistent for argon and CO_2 trials by using pH-adjusted water with $HClO_4$ in the case of argon and neutral water in the case of CO_2.

Materials

All reagents (reagent grade) were obtained from commercial suppliers and used without further purification unless otherwise noted. Anhydrous MeCN, 2-Me THF and CH_2Cl_2 were purchased from Sigma-Aldrich (Sure/Seal). Tetrabutylammonium perchlorate (TBAP, Sigma-Aldrich) was dried under vacuum overnight prior to use. Manganese pentacarbonyl bromide (Strem), 2,2' -bipyridine (bpy, Sigma-Aldrich), Silver cyanide (Sigma-Aldrich) and Silver perchlorate (Sigma-Aldrich) were used as received. Manganese complexes were carefully handled with minimal light exposure. $[Mn(bpy)(CO)_3Br]$ (**2**) and $[Mn(bpy)(CO)_3(MeCN)]PF_6$ were synthesized according to a published methods.[10] Electrolytes were prepared by dissolving TBAP in anhydrous MeCN in a Schlenk flask. The electrolyte was stored under an inert atmosphere and purged immediately prior to use. A 3 mm glassy carbon disk electrode (BASi MF-2012) was used in all electrochemical experiments. Potentials are first referred to an $Ag/AgNO_3$ (10mM) electrode (BASi MW-1085) in 0.1M TBAP/MeCN and then referenced to ferrocene/ferrocenium (Fc/Fc^+). A platinum mesh (~1 cm^2) attached to a platinum wire was used as the counter electrode in all electrochemical measurements. A 15 mL three-neck round-bottom flask was used as the electrochemical cell for CV and a 70 mL four-neck homemade jacketed flask was used for bulk electrolysis. The working electrode and reference electrodes were secured using "mini" Ace-threaded adaptors from Ace-glass (No. 7 and No. 8, respectively). The counter electrode was threaded through a septum, which was then fitted on to one neck of the cell.

Instrumentation

Electrochemical measurements were performed on a Model CHI 760D electrochemical workstation (CH Instruments, Austin, TX). Nuclear magnetic resonance (NMR) spectra were recorded on a Bruker AVANCE spectrometer (500 MHz for ^1H nuclei and 125 MHz for ^{13}C nuclei). Chemical shifts are reported in parts per million (ppm) downfield of tetramethylsilane and are referenced to the solvent residual peak. Fourier transform infrared (FT-IR) spectra were recorded on a Nicolet Model 730 FT-IR spectrometer for gas samples and a Nicolet Model 6700 FT-IR spectrometer equipped with a single-refection diamond ATR attachment for solid samples. UV-vis spectra and photoprocesses were monitored using a Cary 60 UV-vis spectrophotometer (Agilent Technologies). The 365 nm laser output was generated using a Ti-sapphire based laser amplifier (Libra, Coherent) with 1 kHz repetition rate, coupled with Optical Parametric Amplifier (OPeRa, Ultrafast). Pulse duration of the laser was less than 100 fs. X-ray diffraction data were collected with a Bruker Apex II CCD detector using Mo Kα radiation. CO production was analyzed using a 60 °C isothermal method over 5 min on a HP 6890 Gas Chromatograph and TCD with a Molsieve 5A PLOT capillary column (Agilent) running He as the flow gas. H_2 was sampled with an SRI 8610C Gas Chromatograph and TCD with a Molsieve column (HAYESEP D) and Ar flow gas. A 7-min isotherm at 80 °C was employed.

CV Simulations

Simulations of the experimental CV data were performed using DigiElch 4.0 and details are given in the ESI.†

Photochemical reactions

In the control experiment with $^{13}CO_2$, a solution of 8 mL MeCN with 5% H_2O (v/v) and 1mM of the desired complex (**1** or **3**) in a clear borosilicate glass vial sealed with a PTFE/silicone septum (Supleco) was irradiated with a 395 nm LED light (3W) under constant stirring and the headspace was sampled using a gas cell terminated by KBr plates. In photoevolution studies, a solution of 300 μM complex of interest in MeCN was excited at 365 nm laser under constant stirring in a 2 mm wavelength quartz cuvette with screw cap (Firefly) and the absorption spectrum was recorded every 10 min. In the IR studies, the demountable liquid cell was assembled with two CaF_2 windows with 0.1 mm pathlength (PIKE, 162-1100-02). 20 mM sample of interest in MeCN was prepared in the glove box.

Preparation of 1. We mixed **2** (0.29 g, 0.78 mmol), **3** (0.25 g, 0.77 mmol) and $AgClO_4$ (0.17 g, 1.34 mmol) in 25 mL of anhydrous CH_2Cl_2. The resulting solution was stirred in the absence of light at room temperature under Ar. After 3 h the solution was filtered through Celite and concentrated to 3 mL; the product precipitated using Et_2O (20 mL) as a yellow microcrystalline solid (0.42 g, 75%). IR (ATR-IR, cm^{-1}) υ_{CN}:2147 (s), υ_{CO}: 2040 (sh), 2024 (s), 1913 (m). ^1H NMR (500 MHz, CD_2Cl_2) δ 8.81 (d, J = 5.6 Hz, 2H), 8.67 (d, J = 5.5 Hz, 2H), 8.34 (d, J = 8.1 Hz, 2H), 8.28 (d, J = 8.1 Hz, 2H), 8.11 (q, J = 7.3 Hz, 4H), 7.41 (dt, J = 13.1, 6.6 Hz, 4H). ^{13}C NMR (126 MHz, CD_2Cl_2) δ 220.38, 220.07, 217.33, 212.66, 166.99, 155.49, 155.15, 153.16, 153.14, 140.28, 139.83, 127.08, 126.99, 124.00, 123.88.

Preparation of 3. The synthesis of **3** was adapted from a modified literature procedure.[26] A 100 mL Schlenk flask was charged with **2** (0.60 g, 1.60 mmol), AgCN (0.23 g, 1.68 mmol)

and anhydrous CH_2Cl_2 (45 mL). The reaction mixture was stirred in the absence of light at room temperature under argon and monitored by ^{1}H NMR spectroscopy. After 1 h the solution was filtered through Celite, concentrated to 1 mL and then stirred vigorously with 20 mL of a 0.1 M aqueous solution of $Na_2S_2O_3$. The aqueous layer was then extracted with CH_2Cl_2 (20 mL×3), dried with $MgSO_4$ and reduced in vacuo to yield a yellow solid (0.51 g, 98%). IR (ATR-IR, cm^{-1}) υ_{CN}: 2108 (s), υ_{CO}: 2021 (s), 1912 (m). ^{1}H NMR (500 MHz, DMSO-d_6) δ 9.06 (d, J = 5.4 Hz, 2H), 8.69 (d, J = 8.1 Hz, 2H), 8.26 (t, J = 7.8 Hz, 2H), 7.74 (t, J = 6.6 Hz, 2H).

Conflicts of interest

There are no conflicts to declare.

Acknowledgements

The authors acknowledge research funding from the National Science Foundation under Grant No. CHE-1800400. G.D.S. gratefully acknowledges the Division of Chemical Sciences, Geosciences, and Biosciences, Office of Basic Energy Sciences of the U.S. Department of Energy through Grant No. DE-SC0015429.

References

1 P. Huber and M. P. Mills, *The Bottomless Well: The Twilight of Fuel, the Virtue of Waste, and Why We Will Never Run Out of Energy*, Basic Books: New York, Reprint., 2006.
2 E. E. Benson, C. P. Kubiak, A. J. Sathrum and J. M. Smieja, *Chem. Soc. Rev.*, 2008, **38**, 89–99.
3 A. M. Appel, J. E. Bercaw, A. B. Bocarsly, H. Dobbek, D. L. DuBois, M. Dupuis, J. G. Ferry, E. Fujita, R. Hille, P. J. A. Kenis, C. A. Kerfeld, R. H. Morris, C. H. F. Peden, A. R. Portis, S. W. Ragsdale, T. B. Rauchfuss, J. N. H. Reek, L. C. Seefeldt, R. K. Thauer and G. L. Waldrop, *Chem. Rev.*, 2013, **113**, 6621–6658.
4 J. L. White, M. F. Baruch, J. E. Pander, Y. Hu, I. C. Fortmeyer, J. E. Park, T. Zhang, K. Liao, J. Gu, Y. Yan, T. W. Shaw, E. Abelev and A. B. Bocarsly, *Chem. Rev.*, 2015, **115**, 12888–12935.
5 R. Francke, B. Schille and M. Roemelt, *Chem. Rev.*, , DOI:10.1021/acs.chemrev.7b00459.
6 J. Hawecker, J.-M. Lehn and R. Ziessel, *HCA*, 1986, **69**, 1990–2012.
7 N. Elgrishi, M. B. Chambers, X. Wang and M. Fontecave, *Chem. Soc. Rev.*, 2017, **46**, 761–796.
8 A. J. Huckaba, E. A. Sharpe and J. H. Delcamp, *Inorganic Chemistry*, 2016, **55**, 682–690.
9 H. Rao, J. Bonin and M. Robert, *Chemical Communications*, 2017, **53**, 2830–2833.
10 M. Bourrez, F. Molton, S. Chardon-Noblat and A. Deronzier, *Angew. Chem. Int. Ed.*, 2011, **50**, 9903–9906.
11 G. J. Stor, S. L. Morrison, D. J. Stufkens and A. Oskam, *Organometallics*, 1994, **13**, 2641–2650.
12 G. J. Stor, D. J. Stufkens, P. Vernooijs, E. J. Baerends, J. Fraanje and K. Goubitz, *Inorganic Chemistry*, 1995, **34**, 1588–1594.
13 A. Rosa, G. Ricciardi, E. J. Baerends and D. J. Stufkens, *Inorg. Chem.*, 1998, **37**, 6244–6254.
14 F. Hartl, B. D. Rossenaar, G. J. Stor and D. J. Stufkens, *Recl. Trav. Chim. Pays-Bas*, 1995, **114**, 565–570.
15 P. L. Cheung, C. W. Machan, A. Y. S. Malkhasian, J. Agarwal and C. P. Kubiak, *Inorg. Chem.*, 2016, **55**, 3192–3198.
16 J. Agarwal, C. J. S. Iii, T. W. Shaw, J. E. Vandezande, G. F. Majetich, A. B. Bocarsly and H. F. S. Iii, *Dalton Trans.*, 2015, **44**, 2122–2131.
17 H. Takeda, H. Koizumi, K. Okamoto and O. Ishitani, *Chem. Commun.*, 2014, **50**, 1491–1493.
18 M. Stanbury, J.-D. Compain, M. Trejo, P. Smith, E. Gouré and S. Chardon-Noblat, *Electrochimica Acta*, 2017, **240**, 288–299.
19 H. Fei, M. D. Sampson, Y. Lee, C. P. Kubiak and S. M. Cohen, *Inorg. Chem.*, 2015, **54**, 6821–6828.
20 J. Hawecker, J.-M. Lehn and R. Ziessel, *J. Chem. Soc., Chem. Commun.*, 1983, **0**, 536–538.
21 E. E. Benson and C. P. Kubiak, *Chem. Commun.*, 2012, **48**, 7374–7376.
22 C. C. Chang, B. Pfennig and A. B. Bocarsly, *Coordination Chemistry Reviews*, 2000, **208**, 33–45.
23 Y. Wu, B. W. Pfennig, S. L. Sharp, D. R. Ludwig, C. J. Warren, E. P. Vicenzi and A. B. Bocarsly, *Coordination Chemistry Reviews*, 1997, **159**, 245–255.
24 C. J. Adams, K. M. Anderson, N. G. Connelly, E. Llamas-Rey, A. G. Orpen and R. L. Paul, *Dalton Trans.*, 2007, 3609–3622.
25 P. Kurz, B. Probst, B. Spingler and R. Alberto, *Eur. J. Inorg. Chem.*, 2006, **2006**, 2966–2974.
26 G. A. Carriedo, M. C. Crespo, V. Riera, M. L. Valin, D. Moreiras and X. Solans, *Inorganica Chimica Acta*, 1986, **121**, 191–198.
27 F. Scandola, R. Argazzi, C. A. Bignozzi, C. Chiorboli, M. T. Indelli and M. A. Rampi, *Coordination Chemistry Reviews*, 1993, **125**, 283–292.
28 C. Pereira, H. G. Ferreira, M. S. Schultz, J. Milanez, M. Izidoro, P. C. Leme, R. H. A. Santos, M. T. P. Gambardella, E. E. Castellano, B. S. Lima-Neto and R. M. Carlos, *Inorganica Chimica Acta*, 2005, **358**, 3735–3744.
29 B. S. Ault, T. M. Becker, G. Q. Li and M. Orchin, *Spectrochimica Acta Part A: Molecular and Biomolecular Spectroscopy*, 2004, **60**, 2567–2572.
30 H. Hartmann, W. Kaim, M. Wanner, A. Klein, S. Frantz, C. Duboc-Toia, J. Fiedler and S. Záliš, *Inorg. Chem.*, 2003, **42**, 7018–7025.
31 K. Kalyanasundaram, M. Graetzel and M. K. Nazeeruddin, *Inorg. Chem.*, 1992, **31**, 5243–5253.
32 G. A. Carriedo, C. Carriedo, C. Crespo and P. Gómez, *Journal of Organometallic Chemistry*, 1993, **452**, 91–96.
33 K. R. Dunbar and R. A. Heintz, in *Progress in Inorganic Chemistry*, ed. K. D. Karlin, John Wiley & Sons, Inc., 1996, pp. 283–391.
34 D. A. Dows, A. Haim and W. K. Wilmarth, *Journal of Inorganic and Nuclear Chemistry*, 1961, **21**, 33–37.
35 K. Kalyanasundaram, M. Graetzel and M. K. Nazeeruddin, *Inorg. Chem.*, 1992, **31**, 5243–5253.
36 Kurz Philipp, Probst Benjamin, Spingler Bernhard and Alberto Roger, *European Journal of Inorganic Chemistry*, 2006, **2006**, 2966–2974.
37 C. W. Machan, C. J. Stanton, J. E. Vandezande, G. F. Majetich, H. F. Schaefer, C. P. Kubiak and J. Agarwal, *Inorg. Chem.*, 2015, **54**, 8849–8856.
38 R. S. Nicholson and I. Shain, *Anal. Chem.*, 1964, **36**, 706–723.
39 J. Agarwal, T. W. Shaw, H. F. Schaefer and A. B. Bocarsly, *Inorg. Chem.*, 2015, **54**, 5285–5294.
40 M. D. Sampson, A. D. Nguyen, K. A. Grice, C. E. Moore, A. L. Rheingold and C. P. Kubiak, *J. Am. Chem. Soc.*, 2014, **136**, 5460–5471.

41 J. M. Smieja, M. D. Sampson, K. A. Grice, E. E. Benson, J. D. Froehlich and C. P. Kubiak, *Inorg. Chem.*, 2013, **52**, 2484–2491.
42 A. Sinopoli, N. T. La Porte, J. F. Martinez, M. R. Wasielewski and M. Sohail, *Coordination Chemistry Reviews*, 2018, **365**, 60–74.
43 J. E. Pander, A. Fogg and A. B. Bocarsly, *ChemCatChem*, 2016, **8**, 3536–3545.
44 C. Costentin, S. Drouet, M. Robert and J.-M. Savéant, *Science*, 2012, **338**, 90–94.
45 K. A. Grice, N. X. Gu, M. D. Sampson and C. P. Kubiak, *Dalton Trans.*, 2013, **42**, 8498–8503.
46 H. K. Van Dijk, J. Van der Haar, D. J. Stufkens and A. Oskam, *Inorg. Chem.*, 1989, **28**, 75–81.
47 M. W. Kokkes, W. G. J. De Lange, D. J. Stufkens and A. Oskam, *Journal of Organometallic Chemistry*, 1985, **294**, 59–73.
48 T. Van der Graaf, D. J. Stufkens, A. Oskam and K. Goubitz, *Inorg. Chem.*, 1991, **30**, 599–608.
49 D. M. Allen, A. Cox, T. J. Kemp and Q. Sultana, *Inorganica Chimica Acta*, 1977, **21**, 191–194.